ACOUSTIC AND ENTROPIC TRANSFER FUNCTIONS OF A GENERALISED SUBSONIC NOZZLE

Francesca De Domenico, Erwan O. Rolland, Simone Hochgreb
University of Cambridge, Department of Engineering, Cambridge, UK
email: fd314@cam.ac.uk

The knowledge of the acoustic and entropic transfer functions at the boundaries of combustors is crucial to understand the fate of flame-generated pressure perturbations and to predict and prevent the emergence of combustion instabilities. Traditional models often rely on the isentropic assumption for nozzle guide vanes. In real systems, however, pressure losses and local flow recirculations may occur, as evidenced by drops in the static pressure. In this work we relax the isentropic assumption and derive a parametric model to predict the acoustic and entropic transfer functions of generalised convergent-divergent nozzles with subsonic-to-sonic throat conditions in the low frequency domain. By tuning two parameters, this model can retrieve the impedance of three limit cases known from the literature: the isentropic nozzle, the orifice plate and the convergent nozzle duct termination. The generalised model also includes the conversion of entropy to sound through orifice plates and non-isentropic nozzles, yet to be considered in the literature. These analytical results are then compared with the experimental data acquired in the Cambridge Entropy Generator. The comparison highlights the need to correctly account for the losses in the system to properly explain the transfer functions of nozzles, as isentropic predictions differ substantially from the acquired experimental data.
Keyword: Direct and indirect noise, Nozzle, Orifice, Non-isentropic behaviour

1. Introduction

Acoustic perturbations in combustion devices are a topic of increasing interest, particularly as a source of potential instabilities. These acoustic waves are classified as direct and indirect noise. The former arises directly from the heat release rate perturbations in the flame. The latter is generated indirectly from the acceleration of regions of non-uniform temperature, density, composition or vorticity through narrow passages such as turbine nozzle guide vanes. Once created, these acoustic waves (direct and indirect noise) travel through the combustion chamber at the relative speed of sound, until they reach a boundary, where part of their energy is reflected, transmitted and absorbed. The knowledge of the impedance of the boundary is crucial to understand the fate of the impinging acoustic waves [1, 2]. Traditional experimental techniques, such as the two or multi microphone method can be used to characterise the acoustic impedance of the boundaries, however they may be impractical for application in real combustors for long wavelengths. Yet models are needed to predict the entropy-to-sound conversion in nozzles, as there are currently no reliable experimental techniques to measure the conversion of entropic or compositional fluctuations into sound in combustion devices.

Marble and Candel [3] originally developed a one dimensional analytical model to predict the transfer function of isentropic compact nozzles, deriving expressions for the magnitude of reflected and transmitted direct and indirect noise in the low frequency limit (*i.e.* for wavelengths much longer than the nozzle). The isentropic assumption implies that no pressure losses occur across the nozzle. In real situations, however, this may not be the case: losses and recirculation zones often appear at nozzles/turbine blades [4], so that the flow is not isentropic. Durrieu *et al.* [5] introduced an analytical model to describe the low frequency acoustic transfer function of a non-isentropic jump such as an

orifice plate. Howe [6] and Bechert [7] modelled the reflective acoustic properties of a subsonic nozzle that terminates a duct, where the flow expands non-isentropically into the atmosphere as a jet. However, neither of these authors included information on the entropy-to-sound conversion in their models.

In this work, we introduce a model to predict the acoustic and entropic transfer functions of a generalised nozzle with flows from subsonic to sonic conditions, and demonstrate how the generalised transfer functions reduce to previously derived limit cases for: an isentropic convergent-divergent nozzle, an orifice plate and a convergent nozzle duct termination. We demonstrate how the non-isentropic transfer functions differ significantly from the isentropic predictions. The analytical non-isentropic predictions are then compared with experimental data obtained with the Cambridge Entropy Generator [8]. The experimental reflection and transmission coefficients are in good agreement with the non-isentropic model, which differs substantially from the isentropic transfer functions.
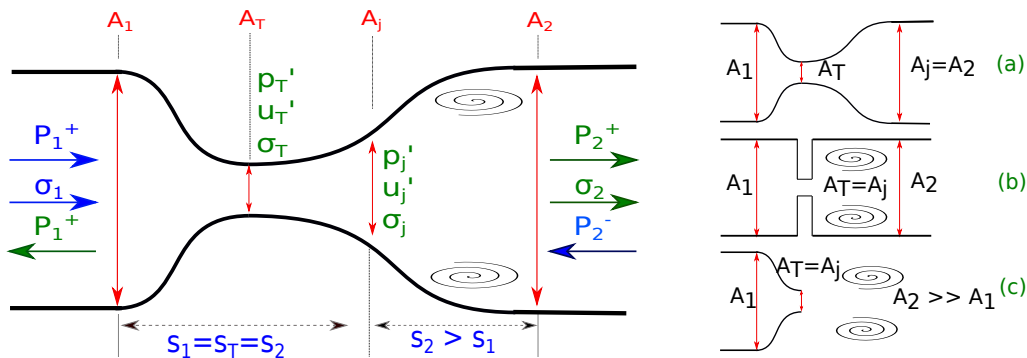
2. Model

Figure 1: Schematic of the generalised nozzle. Limit cases: (a) isentropic convergent/divergent nozzle; (b) orifice plate; (c) convergent-nozzle end termination.

In this section, we introduce a parametric analytical model which predicts the acoustic and entropic transfer functions of a generalised subsonic and sonic nozzle (Fig. 2). The flow through the nozzle is assumed to be quasi-one-dimensional: all the flow properties are uniform across any cross sections of the nozzle. The wavelengths of the perturbations are longer than the discontinuity, so the model is developed in the low-frequency limit (quasi-steady assumption).

The nozzle is divided into four nodes, as shown in figure 2. A_1 and A_2 are respectively the inlet and outlet areas. A_T is the throat area, considered as the smallest area the flow passes through (a vena contracta factor $\Gamma = 1$ is assumed for now). The flow is modelled as isentropic from the inlet to an area section j located in the divergent between the throat and the exit of the nozzle: beyond A_j, the flow detaches from the wall, recirculation areas and vortices appear, thus the isentropic assumption is no longer valid. The separation causes pressure losses and absorption of acoustic energy. The position of A_j can be varied through the divergent as an indicator of the *level of anisentropicity* of the nozzle: the closest A_j is to A_T, the highest these losses become. If $A_j = A_T$ (Fig. 2(b), the orifice plate limit [5] is recalled, in the form of the condition furthest from isentropicity. For $A_j = A_2$ (Fig 2(b)), there is no separation in the nozzle, and the isentropic convergent-divergent nozzle model [3] is recovered. Therefore, a real convergent-divergent nozzle is expected to behave somewhere in between these two limit cases ($A_T < A_j < A_2$). Finally, when $A_j = A_T$ and $A_2 \to \infty$, the convergent nozzle duct termination limit is obtained [6, 7] (Fig. 2(c)). The four relative areas are needed to fully describe the *generalised nozzle* and capture the limit cases: the generalised subsonic nozzle is no longer modelled as a compact jump, and the internal flow behavior becomes a parameter dependent on the nozzle geometry and the corresponding flow dissipations.

We define the pressure p', velocity u', density ρ' and entropy σ as perturbations relative to the

mean flow, where:

$$p' = P^+ e^{-ik^+x} + P^- e^{ik^-x}; \qquad u' = \frac{P^+ e^{-ik^+x} - P^- e^{ik^-x}}{\rho c}; \qquad \sigma = p' - c^2 \rho' \qquad (1)$$

where P is the amplitude of the acoustic wave, the superscripts $^+$ and $^-$ correspond to the downstream and upstream travelling wave intensities, respectively, and k are the corresponding wavenumbers. The density is ρ and the speed of sound is c.

2.1 Conservation equations for inviscid flows

The governing equations for a steady quasi-one-dimensional flow are obtained by applying the integral form of the conservation equations to a variable area-control volume, delimited by sections A_m and A_n. The flow is assumed as adiabatic, without any external heat, mass or momentum additions. Three equations are needed to fully characterise the changes in the flow properties between these two sections.

The integral conservation laws governing the flow behaviour are [9]:

Mass conservation: $$\rho_m A_m u_m = \rho_n A_n u_n \qquad (2a)$$

Total enthalpy conservation : $$\frac{1}{2}u_m^2 + c_p T_m = \frac{1}{2}u_n^2 + c_p T_n \qquad (2b)$$

Momentum conservation : $$p_m + \rho_m u_m^2 + \frac{1}{A_m}\int_m^n A \, \mathrm{d}P = p_n \frac{A_n}{A_m} + \rho_n u_n^2 \frac{A_n}{A_m} \qquad (2c)$$

For an isentropic flow, the total enthalpy and momentum conservation are equivalent. In this case, the additional condition needed to describe the flow is the entropy conservation, which leads to:

$$p_m/\rho_m^\gamma = p_n/\rho_n^\gamma \qquad (3)$$

This is equivalent to a statement that there is a full pressure recovery in the nozzle. In contrast, losses in pressure occur when the flow separates. For the case of an orifice plate, assuming that the flow exits from the separation section in the throat A_T (assuming a vena contracta factor $\Gamma = 1$) as a jet oriented purely in the axial direction, with transverse pressure constant along this separation plane, the momentum conservation Eq. 2c becomes: $A_2(p_T - p_2) + \rho_T u_T^2 A_T = \rho_2 u_2^2 A_2$ [5, 4]. A *real nozzle* is expected to display an intermediate behaviour between the most non-isentropic case (the orifice plate) and the fully isentropic nozzle. Here we parametrise the *level of anisentropicity* by a flow detachment area A_j located in the divergent, or equivalently by the ratio $\beta = A_j/A_T$. The generalised momentum conservation equation for the non-isentropic nozzle between the sections A_j and A_2 becomes:

$$A_2(p_j - p_2) + \rho_j u_j^2 A_j = \rho_2 u_2^2 A_2 \qquad A_T \le A_j \le A_2 \qquad (4)$$

As demonstrated further onwards, the upstream static pressure increase versus the mass flow rate can equally be used as an indicator of the *level of anisentropicity* the nozzle: the higher the dissipation, the higher the pressure drop across the nozzle, leading to a higher pressure increase upstream of the convergent section for a given flow rate. The actual value A_j is expected to vary for different mass flow rates, as dissipative effects depend on flow parameters such as the Reynolds number, which varies when the mass flow rate is increased. For zero dissipation, there is a full pressure recovery downstream of the throat (e.g. if $A_2 = A_1$ in subsonic conditions, the same static pressure p_1 and p_2 should be measured upstream and downstream of the nozzle).

To fully describe a real nozzle, the assumption $\Gamma = 1$ should be relaxed and the Mach number dependency of the vena contracta factor should be implemented ($\Gamma = \Gamma(M)$ [5]).

2.2 Small perturbations on the base flow

In this section, we introduce the acoustic and entropic transfer functions for the *generalised nozzle* of figure 2. Small perturbations are superposed on the mean flow quantities in the integral conservation equations 2. The detailed derivation of the perturbed equations is not described here, as it can be found in [3] for the isentropic case and in [5] for the non-isentropic case.

The generalised nozzle is divided into four nodes, so 12 variables are needed to fully determine the system. Three are the imposed impinging quantities (blue arrows in figure 2): the incoming acoustic and entropy perturbations from upstream (P_1^+ and σ_1) and the incoming acoustic wave from downstream (P_2^-). The remaining 9 unknown are determined with 9 equations, obtaining a 9x9 transfer function matrix (Eq. 5, for $P_2^- = 0$). A discussion of the generalised nozzle transfer functions follows below.

$$
\begin{bmatrix}
-\frac{1-M_1}{c_1} & -\frac{A_2}{A_1}\frac{1+M_2}{c_2} & \frac{A_2}{A_1}\frac{M_2}{c_2} & 0 & 0 & 0 & 0 & 0 & 0 \\
-\frac{1-M_1}{c_1} & 0 & 0 & -\frac{A_j}{A_1}\frac{1}{c_j}M_j & -\frac{A_j}{A_1}\rho_j & \frac{A_j}{A_1}c_jM_j & 0 & 0 & 0 \\
-\frac{1-M_1}{c_1} & 0 & 0 & 0 & 0 & 0 & -\frac{A_T}{A_1}\frac{1}{c_T}M_T & -\frac{A_T}{A_1}\rho_T+\frac{A_T}{A_1}\frac{1}{c_T}M_T & 0 \\
\frac{1-M_1}{\rho_1} & -\frac{1+M_2}{\rho_2} & -\frac{1}{\gamma-1}\frac{1}{\rho_2} & 0 & 0 & 0 & 0 & 0 & 0 \\
\frac{1-M_1}{\rho_1} & 0 & 0 & -\frac{1}{\rho_j} & -c_jM_j & -\frac{1}{\gamma-1}\frac{1}{\rho_j} & 0 & 0 & 0 \\
\frac{1-M_1}{\rho_1} & 0 & 0 & 0 & 0 & 0 & -\frac{1}{\rho_T} & -c_TM_T & --\frac{1}{\gamma-1}\frac{1}{\rho_T} \\
0 & -(1+M_2)^2 & M_2^2 & (1+\frac{A_j}{A_2}M_j^2)\,2\frac{A_j}{A_2}\rho_jM_jc_j & -M_j^2\frac{A_j}{A_2} & 0 & 0 & 0 \\
0 & 0 & 0 & 0 & 0 & \frac{1}{\rho_j^\gamma} & 0 & 0 & 0 \\
0 & 0 & 0 & 0 & 0 & 0 & 0 & 0 & \frac{1}{\rho_T^\gamma}
\end{bmatrix}
\begin{bmatrix}
P_1^- \\ P_2^+ \\ \sigma_2 \\ p_j' \\ u_j' \\ \sigma_j \\ p_T' \\ u_T' \\ \sigma_T
\end{bmatrix}
=
\begin{bmatrix}
-\frac{1+M_1}{c_1} \\ -\frac{1+M_1}{c_1} \\ -\frac{1+M_1}{c_1} \\ -\frac{1+M_1}{\rho_1} \\ -\frac{1+M_1}{\rho_1} \\ -\frac{1+M_1}{\rho_1} \\ 0 \\ 0 \\ 0
\end{bmatrix}
P_1^+ +
\begin{bmatrix}
\frac{M_1}{c_1} \\ \frac{M_1}{c_1} \\ \frac{M_1}{c_1} \\ -\frac{1}{\gamma-1}\frac{1}{\rho_1} \\ -\frac{1}{\gamma-1}\frac{1}{\rho_1} \\ -\frac{1}{\gamma-1}\frac{1}{\rho_1} \\ 0 \\ \frac{1}{\rho_1\gamma} \\ \frac{1}{\rho_1\gamma}
\end{bmatrix}
\sigma_1
$$

(5)

2.2.1 Transfer functions of the generalised convergent-divergent nozzle

Figure 2 shows the acoustic (R, T) and entropic (S_R, S_T) transfer functions of the generalised nozzle (Eq. 5), obtained by varying the value of $\beta = A_j/A_T$. These coefficients are defined as follows, where the subscript $_s$ refers to the acoustic waves generated from the acceleration of the entropy waves:

$$
R = \frac{P_1^-}{P_1^+}; \qquad T = \frac{P_2^+}{P_1^+}; \qquad S_R = \frac{P_{(1,s)}^-}{\sigma_1}; \qquad S_T = \frac{P_{(2,s)}^+}{\sigma_1}
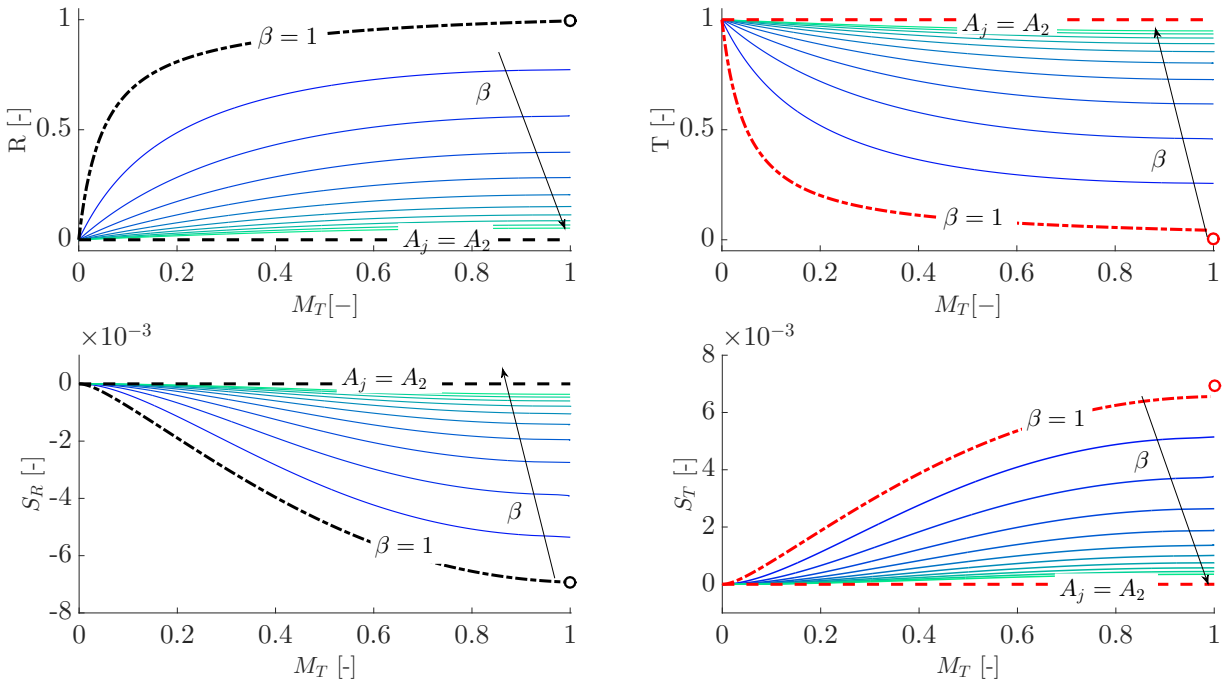\tag{6}
$$

Figure 2: Acoustic (R, T) and entropic (S_R, S_T) transfer functions for the generalised convergent-divergent nozzle. Dashed lines: isentropic subsonic predictions [3] ($A_j = A_2$); circular markers: isentropic choked predictions [3]; dashed-dotted lines: orifice plate model [5] ($A_j = A_T$; $\beta = 1$), solid lines: results from Eq. 5 for values of $\beta = A_j/A_T = [2, 3, 4, 5, 6, 7, 8, 9, 10]$.

These transfer functions are plotted by using the dimensions of the Cambridge Entropy Generator [8] ($d_1 = d_2 = 42.6$ mm; $d_T = 6.6$ mm). The corresponding transfer functions derived for the isentropic nozzle ($A_j = A_2$; $\beta = 41.66$) in subsonic (dashed lines) and sonic (circular markers) con-

ditions are highlighted [3]. The dashed-dotted lines correspond to the reflectivity and transmissivity of the orifice plate assuming a vena contracta factor $\Gamma = 1$ [5] ($A_T = A_j$; $\beta = 1$).

In the generalised formulation of Eq. 5, if $A_j = A_2$, the isentropic nozzle transfer functions [3] are retrieved for subsonic conditions. Instead, if $A_j = A_T$ ($\beta = 1$), the orifice plate model is recalled. From Fig. 2 it can be noticed that, while the orifice plate model predicts a continuous behaviour of the reflectivity and transmissivity of the jump from subsonic to sonic conditions, the isentropic coefficients have a discontinuity at $M = 1$. The acoustic and entropic reflection coefficients at the choking condition are the same for the isentropic nozzle and the orifice plate, as the the flow before the throat is modelled as isentropic in both cases, and no information about the downstream flow travels upstream of a choked point. The non-isentropic transmissivity at choking condition, instead, is lower than the isentropic value, as losses in the divergent section dissipate part of the acoustic energy. The orifice plate and the isentropic nozzle represent two opposite limit cases, so a real nozzle in subsonic condition is expected behave somewhere in between. The solid lines in figure 2 are obtained by varying β. For $\beta \simeq 1$ ($A_j \simeq A_T$), the reflections coefficients are highly influenced by the particular value A_j, i.e. by the dissipations. When $\beta \simeq 10$, the reflection coefficients are practically isentropic. It is interesting to notice the opposite behaviour between isentropic and non isentropic nozzles: in terms of direct noise, the more non isentropic the nozzle is (the higher the dissipation in the nozzle), the higher is the reflectivity and the lower is the transmissivity in terms of direct noise. Conversely, while *zero* indirect noise is predicted under isentropic conditions either upstream or downstream of the nozzle, both reflected and transmitted indirect (entropic) noise are non negligible for the non-isentropic nozzle.

2.2.2 Duct terminated with a subsonic convergent nozzle

Figure 3 shows the acoustic (a) and entropic (b) transfer functions for a subsonic purely convergent nozzle with a sudden expansion to the atmosphere at the end. The solid lines represent the transmissivity (red) and reflectivity (black) obtained from the transfer matrix (Eq. 5) for $A_2 \to \infty$ and $A_j = A_T$. The acoustic reflection coefficient derived from an energy balance in previous literature is added [6, 7, 5] (Green line, Eq. (39) in [5]). This prediction from [5] overlaps perfectly with the analytical reflection coefficient obtained from Eq. 5.
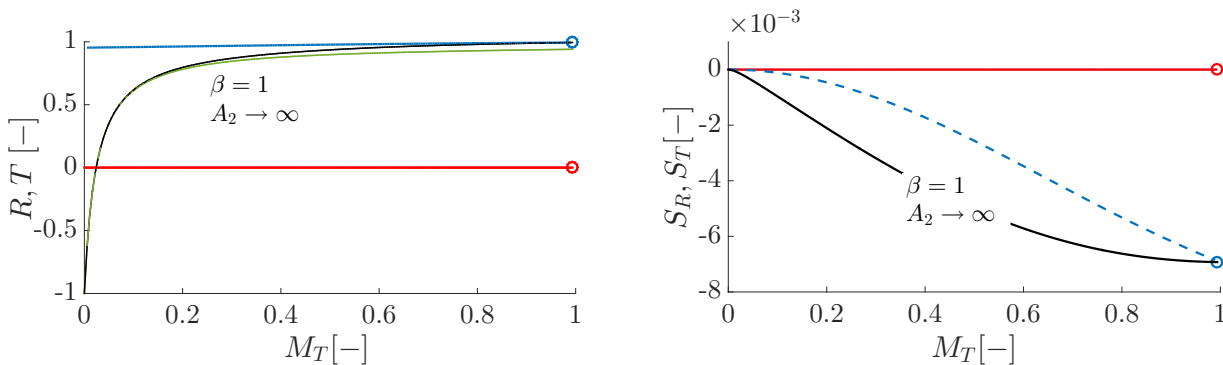

Figure 3: Acoustic (a) and entropic (b) transfer functions of the convergent nozzle. Blue lines: isentropic predictions; solid black (R and S_R) and red (T and S_T) lines: results of the transfer function Eq. 5 ($A_T = A_j$, $\beta = 1$, $A_2 \to \infty$); green line: direct noise reflection coefficient predicted from Durrieu (Eq. (39) in [5])

The blue lines, instead, represent the acoustic and entropic transfer functions calculated using the isentropic subsonic formula [3] between the Mach number M_1 and the throat Mach number M_T. These isentropic results differ substantially from the model of the convergent nozzle expanding into a jet, both for the direct and the indirect noise: the isentropic equation from [3] over-predicts the reflected acoustic wave and under-predicts the generated indirect noise. Although the flow through the convergent nozzle can be modelled as isentropic, the non-isentropic expansion of the jet downstream

of the throat can not be neglected.

3. Experimental validation
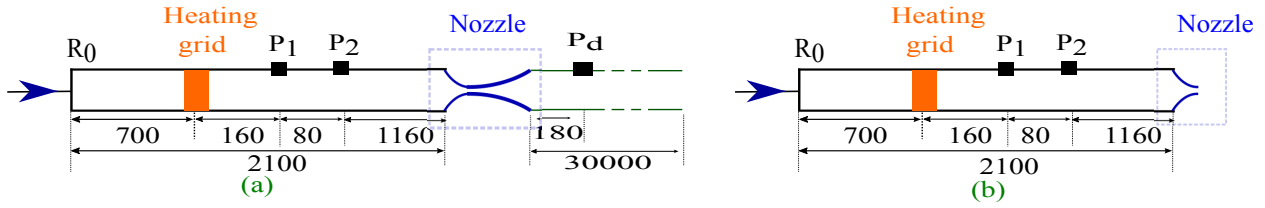
3.1 Set-up description

Figure 4: Schematic of the experimental rig: (a) convergent-divergent nozzle configuration; (b) orifice-terminated duct. Dimensions in mm. Not to scale.

The experimental set-up used to validate the analytical results is briefly described in this section (Fig. 4). A more detailed description can be found in [8, 10]. Air flows through a 42.6 mm diameter tube at a controlled rate and is accelerated via a convergent/divergent nozzle (a) or an orifice plate (b). A heating device is located 1.4 m before the acceleration point. Current is pulsed into this heating module for $t_p = 0.1$ s, generating acoustic pulses (*direct noise*) and hot spots. The hot spots are then advected with the mean flow and, when accelerated, they produce *indirect noise*. The convergent-divergent nozzle and the orifice plate have a throat diameter of 6.6 mm. The angles of the convergent and divergent are $\alpha_C = 40°$ and $\alpha_D = 4.5°$, respectively. A 30-meter-long tube (d = 45 mm) is attached downstream of the convergent-divergent nozzle to isolate the acoustic waves transmitted through the nozzle: the round-trip time for a sound wave to reflect back off the end of the tube is $t_a = 2L/c \simeq 0.2$ s [8], so that the downstream end is anechoic for $t < t_a$. Dynamic pressure measurements are performed upstream and downstream of the nozzle, via flush-mounted piezoresistive pressure transducers (3 Kulite XTE 190M, 1 Kulite XT-140M), at locations indicated in figure 4.

3.2 Acoustic transfer functions of a non-isentropic convergent-divergent nozzle

Figure 5 shows the analytical and experimental predictions for the acoustic reflectivity (black) and transmissivity (red) of the convergent/divergent nozzle (Fig. 4(a)). The reverberation of the acoustic waves (multiple reflections at the boundaries) needs to be taken into account in order to correctly interpret the experimental data. The peaks of the upstream and downstream acoustic oscillations are used to evaluate the transmitted and reflected acoustic waves. As the duct length ($L_d = 2.1$ m) is shorter than the acoustic wavelength ($L_d << \lambda = c/f$), the experimental coefficients R, T (markers in figure 5) can be evaluated from the acquired upstream (u) and downstream (d) pressure peaks using the following relations [10, 11]:

$$\frac{(p'_{max})_d}{(p'_{max})_u} \simeq \frac{\frac{T(P^+ + R_0 P^-)_{max}}{1 - R_0 R}}{\frac{(P^+ + R_0 P^-)_{max}(1+R)}{1 - R_0 R}} = \frac{T}{1 + R}; \qquad (p'_{max})_u \simeq \frac{(P^+ + R_u P^-)_{max}(1 + R)}{1 - R_0 R} \qquad (7)$$

where P^+ and P^- are the downstream and upstream acoustic waves generated from the heating grid. In the current experiment, the value R_0 (inlet reflection coefficient of the duct) is shown to be 0.97 [11]. The amplitude of the travelling wave ($P^+ + R_0 P^-$) is obtained from a separate experiment (further details can be found in [10]).

Figure 5(b) shows the mean absolute upstream pressure in the duct as a function of upstream duct velocity, calculated using the geometric dimensions of the rig. The experimental values of pressure show that the geometric value of the area ratio does not entirely capture the behaviour of the pressure for higher flow rates. This can be explained by the fact that the flow detaches from the wall at the throat, leading to a vena contracta factor Γ lower than unity, and an effective area smaller than A_T.
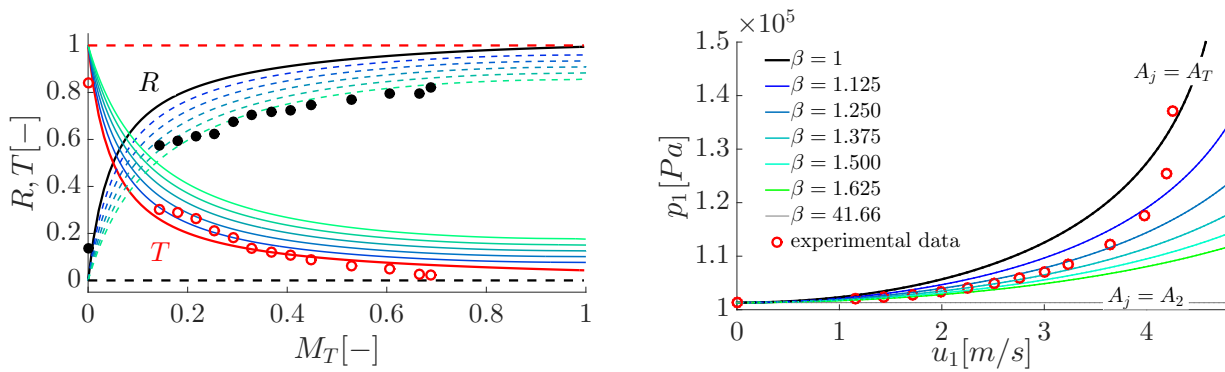
Figure 5: (a) Direct noise reflection (black) and transmission (red) coefficients for the convergent-divergent nozzle: experimental data (markers); isentropic nozzle model (dashed black and red lines [3]), orifice plate model (solid black and red lines [5]); *generalised nozzle model* (solid lines for T, dashed lines for R) obtained for different A_j/A_T. (b) Mean absolute upstream pressure versus upstream duct velocity for the different ratios A_j/A_T; markers: experimental values.

This shows that the variability of the vena contracta factor ($\Gamma = \Gamma(M) \neq 1$) should also be implemented in the model to fully capture the behaviour a real nozzle. The perturbations are also affected by the *level of anisentropicity*, as the nozzle transfer functions display an intermediate behaviour between an isentropic nozzle and a non-isentropic orifice plate.

3.3 Acoustic and entropic transfer functions of the orifice terminated duct

Figure 6 shows the comparison between the experimental direct (a) and indirect noise (b) transfer functions (markers) and the analytical results (lines) obtained for the subsonic, orifice-terminated duct [8, 11]. In a previous investigation it was shown that the subsonic orifice plate behaves as a convergent nozzle in terms of direct and indirect noise generated [10]. Yet the isentropic transfer functions (blue lines) over-predict the direct noise and under-predict the indirect noise generated upstream of the orifice, respectively. Instead, the generalised nozzle transfer function (Eq. 5) matches the experimental data well, both for the direct and the indirect noise. In the previous literature, models and experimental validation of the acoustic reflection coefficient of non isentropic jumps can be found (e.g. [5]). However, figure 6 is the first experimental evidence that isolates the reflected indirect noise arising from a non isentropic jump. In particular, it emphasises how a non-isentropic model is needed to evaluate the entropy-to-sound conversion in a subsonic nozzle, as the isentropic model underestimates the generated entropic sound.
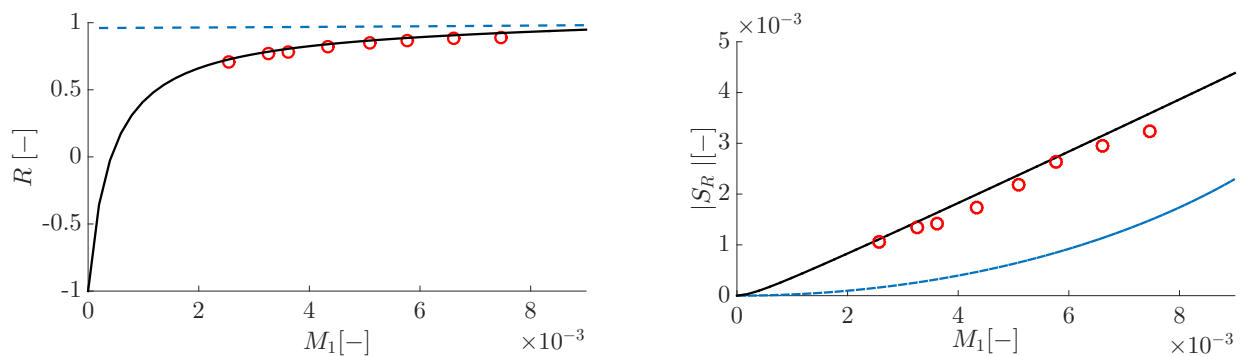

Figure 6: Acoustic (a) and entropic (b) reflection coefficients of the convergent-nozzle-duct termination [8, 11]: experimental data (markers), isentropic predictions (blue lines) and predictions from the generalised nozzle transfer function (Eq. 5, solid black lines).

4.   Conclusions

We introduce a parametric model to predict the acoustic and entropic transfer functions of a generalised nozzle in the low frequency domain. This model extends the isentropic formulation to non-isentropic flow behaviour in subsonic-to-sonic throat conditions. By tuning two parameters (the effective area ratio corresponding to the irreversibility and the area downstream of the nozzle), the generalised model can retrieve the acoustic transfer functions of three limit cases known from the literature: the isentropic nozzle, the orifice plate and the convergent nozzle duct termination. To these, our model adds the entropy-to-sound conversion under dissipative conditions, which was not previously investigated. We then compared the analytical predictions from our generalised model with the experimental data acquired from the Cambridge Entropy Generator.

Very good agreement can be found between the experimental acoustic reflectivity and transmissivity in the non-isentropic convergent-divergent nozzle and the analytical predictions for a non isentropic jump. Instead, the isentropic theory not only does not capture the experimental data, but also shows incompatible trends. The entropy-to-sound conversion is analysed in the convergent nozzle duct termination. Direct and indirect noise are separated in the acquired pressure trace, and the experimental transfer functions are compared with the analytical models. The non-isentropic theory is needed to explain the data, as the isentropic predictions do not capture the experimental transfer functions. These results emphasise how the dissipation in a system should be accounted for to correctly predict the nozzle behaviour. If isentropic models are used to characterise dissipative flows, wrong conclusions can be obtained about the origin of the noise. In particular, the indirect noise in subsonic conditions is highly underestimated by the isentropic theory. These considerations become crucial in understanding how to attribute and remedy instabilities in real systems, where direct and indirect noise are mixed in the acquired pressure trace. If inappropriate transfer functions are applied to de-convolute direct and indirect noise in the pressure data, the origin of the oscillations may be misunderstood.

References

1. Dowling, A. P. and Mahmoudi, Y. Combustion Noise, *Proceedings of the Combustion Institute*, **35** (1), 65–100, (2015).
2. Goh, C. S. and Morgans, A. S. The Influence of Entropy Waves on the Thermoacoustic Stability of a Model Combustor, *Combustion Science and Technology*, (July 2015), 120816123400009, (2013).
3. Marble, F. and Candel, S. Acoustic disturbance from gas non-uniformities convected through a nozzle, *Journal of Sound and Vibration*, **55** (2), 225–243, (1977).
4. Lieuwen, T., *Unsteady Combustion Physics*, Cambridge University Press (2012).
5. Durrieu, P., Hofmans, G., Ajello, G., Boot, R., Aurégan, Y., Hirschberg, A. and Peters, M. C. Quasisteady aero-acoustic response of orifices., *The Journal of the Acoustical Society of America*, **110** (4), 1859–1872, (2001).
6. Howe, M. S. Attenuation of sound in a low Mach number nozzle flow, *Journal of Fluid Mechanics*, **91** (1979), (2017).
7. Bechert, D. Sound absorption caused by vorticity shedding, demonstrated with a jet flow, *Journal of Sound and Vibration*, **70** (79), 389–405, (1980).
8. De Domenico, F., Rolland, E. O. and Hochgreb, S. Detection of direct and indirect noise generated by synthetic hot spots in a duct, *Journal of Sound and Vibration*, (2017).
9. Anderson, J., *Modern Compressible Flow with Historical Perspective*, McGraw-Hill, third edn. (2004).
10. De Domenico, F., Rolland, E. O. and Hochgreb, S. Measurements of the effect of boundary conditions on upstream and downstream noise arising from entropy spots, *Proceedings of ASME Turbo Expo 2017 GT2017*, (2017).
11. Rolland, E. O., De Domenico, F. and Hochgreb, S. Theory and application of reverberated direct and indirect noise, *Journal of Fluid Mechanics*, (2017).